

Investigations of active interrogation techniques to detect special nuclear material in maritime environments: Standoff interrogation of small- and medium-sized cargo ships



Thomas M. Miller*, Bruce W. Patton, Brandon R. Grogan, James J. Henkel, Brian D. Murphy, Jeffrey O. Johnson, John T. Mihalczo

Oak Ridge National Laboratory, P.O. Box 2008, Oak Ridge, TN 37831, USA

ARTICLE INFO

Article history:

Received 7 March 2013

Received in revised form 4 July 2013

Available online 31 August 2013

Keywords:

Active interrogation

Nonproliferation

Nuclear materials detection

Standoff interrogation

Monte Carlo

Variance reduction

ABSTRACT

In this work, several active interrogation (AI) sources are evaluated to determine their usefulness in detecting the presence of special nuclear material (SNM) in fishing trawlers, small cargo transport ships, and luxury yachts at large standoff distances from the AI source and detector. This evaluation is performed via computational analysis applying Monte Carlo methods with advanced variance reduction techniques. The goal is to determine the AI source strength required to detect the presence of SNM. The general conclusion of this study is that AI is not reliable when SNM is heavily shielded and not tightly coupled geometrically with the source and detector, to the point that AI should not be considered a via interrogation option in these scenarios. More specifically, when SNM is shielded by hydrogenous material large AI source strengths are required if detection is based on neutrons, which is not surprising. However, if the SNM is shielded by high-Z material the required AI source strengths are not significantly different if detection is based on neutrons or photons, which is somewhat surprising. Furthermore, some of the required AI source strengths that were calculated are very large. These results coupled with the realities of two ships moving independently at sea and other assumptions made during this analysis make the use of standoff AI in the maritime environment impractical.

© 2013 Elsevier B.V. All rights reserved.

1. Introduction

This work examines an aspect of the problem posed by the threat of the surreptitious transport of special nuclear materials (SNM) in the marine environment. In particular, we focus on radiation-sensing technologies that might be useful in the detection, via remote monitoring, of significant quantities of fissile materials when sequestered in maritime vessels. The technology investigated in this work is active interrogation (AI), which uses an active source to create a signal, such as fission, that can be detected. Because the general area of maritime detection and interdiction of SNM is complex and beyond the scope of a single article, this paper focuses on one specific scenario of interest: the “high seas” ship-to-ship detection of SNM via AI. The scenario involves the search/scan of a vessel from nearby, without boarding it (i.e., a ship-to-ship interdiction and search from a few tens of meters). For the current investigation, the threat basis is restricted to include only fishing trawlers, small cargo transport ships (e.g., break-bulk carriers), and luxury yachts, which are all assumed to have steel hulls.

The goal is to determine the source strength required of different AI sources to detect the presence of SNM in these types of ships. This examination is performed completely via computational analysis applying Monte Carlo methods with advanced variance reduction techniques due to the difficulty and expense of performing experimental measurements of the same type.

AI has been evaluated experimentally and computationally in previous work [1–6]. Refs. [5] and [6] provide a comprehensive review of the efforts focused on detecting SNM. For the purposes of most of the past work, the geometry was lightly shielded and spatially tightly coupled. At most, the contents of one standard cargo container (2.44 m × 2.60 m × 6.10 m) were interrogated, and the source and detector were both within a few meters of the SNM. AI scenarios in which the geometry is more heavily shielded and/or at larger standoff distances will require larger source intensities, larger detector surface areas (bigger detectors or more detectors), greater detector efficiencies, longer count times, or some combination of these.

The target break-bulk carrier represents the largest vessel considered in this investigation. These ships are typically 61–152 m in length and carry bulk cargo (dry or liquid) or break bulk cargo (cargo with individually handled pieces). In some instances they carry

* Corresponding author. Tel.: +1 865 574 9909; fax: +1 865 576 3513.

E-mail address: millerlm@ornl.gov (T.M. Miller).

a limited number of containers on deck. Many have cranes onboard for loading and unloading operations, giving them access to smaller seaports and river ports that do not have significant loading/unloading infrastructure.

The target fishing trawlers range from 24 m to 37 m in length and are typical of fishing vessels that leave from and return to the same port after an extended fishing trip. For the luxury yacht, the target vessel is a motorized yacht from 30 m to 46 m in length.

The interrogation sources are co-located with computational particle tallies, which represent radiation detectors, at a fixed distance from the ship being interrogated. For all of these vessels, the cargo loadings are assumed to be homogenized representations of typical cargo. More realistic heterogeneous cargo could create streaming paths, but these are not modeled due to the infinite number of possible configurations. The threat object used is a 25-kg sphere of highly enriched uranium (HEU), which represents the International Atomic Energy Agency standard for a significant quantity of HEU [7]. The threat object is placed at several different locations in each ship, and Monte Carlo methods are used to calculate interrogating source strengths required to detect the presence of the threat object in each location.

2. Ship geometry models and threat object locations

To begin this investigation, computational models of a luxury yacht, a break-bulk carrier, and a fishing trawler were built. The models have been developed primarily for use with the MCNPX radiation transport code version 2.6.0, which was the primary computational tool used in this investigation [8]. The model of the luxury yacht is based on the Ocean Alexander 98 Motoryacht [9], and the fishing trawler model is based on the Stark Brothers LTD SB-ST19 Steel Trawler [10]. The break-bulk cargo carrier model is based on the SS Cape Chalmers, which is located at the Federal Law Enforcement Training Center in Charleston, South Carolina, USA [11].

The evaluation of AI sources with the MCNPX luxury yacht model was limited to three different areas: the engine room, the liquid storage tanks, and the “cabin type rooms”, which are all labeled in images of the MCNPX geometry in Figs. 1 and 2 and are colored consistently in both figures. Cabin type rooms include the galley, cabin, and head. These rooms were lumped together because they largely consist of air. These three areas were selected because they bracket all the rooms/shielding materials onboard the luxury yacht. The engine room represents a high-Z material or shield, which maybe problematic for AI photon sources. The liquid storage tanks represent a hydrogenous material or shield, which maybe problematic for AI neutron sources. The cabin-type rooms are typical representations of most areas on the luxury

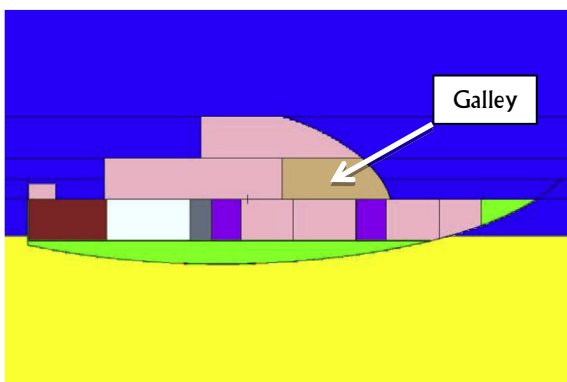


Fig. 1. Elevation view showing a cross section of the MCNPX yacht model.

yacht outside the engine room and liquid storage tanks. Inside each of these three areas, the assessment of AI sources was performed with the threat object in two different locations. The first location was at the centerline of the yacht and the second location was 1 m inside the hull. All six locations were on the lower deck, but 1 m above the waterline; they are marked (approximately) in Fig. 2. In Fig. 2 the yacht centerline locations are marked by red dots and the locations 1 m inside the hull are marked by blue dots. The centerline of the yacht and 1 m inside the hull were used because those locations represent the deepest and shallowest possible penetrations, respectively, that an AI source would have to make. The distance from the side of the yacht to the centerline of the ship varies, but was between 2.7 and 2.9 m for the locations considered in this investigation. Results from those locations can also be used to assess a fishing trawler because a fishing trawler will also have an engine room and cabin-type rooms. However, a yacht does not have a large hold that may be filled with fish and ice.

The MCNPX fishing trawler model is based on a version originally obtained from Los Alamos National Laboratory [12], which was updated for this effort. Images of the Oak Ridge fishing trawler model are shown in Fig. 3 and 4. The freezer hold of the fishing trawler is considered the most likely region of concern with regard to the illicit transport of SNM. This is primarily because the volume is large and the hydrogenous material provides substantial neutron shielding. Other possible SNM hiding locations of concern are the diesel fuel tank and the engine room. The diesel fuel tank is also a volume filled with hydrogenous material. Although it is not as large as the freezer hold, the diesel tank is always below the waterline, which presents an additional amount of neutron shielding. The engine room is also always below the waterline. It is considerably smaller than the freezer hold, but it contains a large amount of high-Z material, which provides substantial photon shielding. The engine compartment and liquid storage tank of the luxury yacht

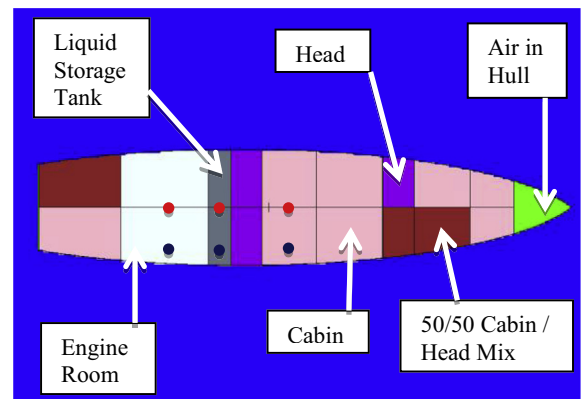


Fig. 2. Plan view of lower deck of the MCNPX model.

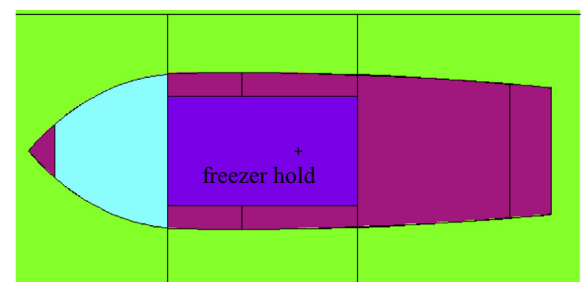


Fig. 3. A plan view of the fishing trawler MCNPX model.

studied in this project are comparable to the engine compartment and diesel tank of the fishing trawler. Therefore, the only location evaluated during this study with the fishing trawler model was the freezer hold. Similar to its placement on the luxury yacht, the HEU threat object was placed at two locations: along the centerline of the trawler and 1 m inside the hull of the ship and 0.5 m above the waterline in both locations. The distance from the side of the trawler to the centerline is 2 m.

In the simulations for this study, all interrogation sources, threat objects, and detectors were located above the waterline, which is a significant assumption for the trawler model. Fig. 4 illustrates that a threat object in the trawler's freezer would likely be below the waterline. The waterline and draft (the amount of ship below the waterline) of the trawler in Fig. 4 is representative of typical fishing trawlers of this size, therefore the draft of the fishing trawler model was artificially reduced to ensure the threat object at the center of the freezer hold was above the waterline during this analysis. If the threat object is inside a full freezer hold below the waterline, there is additional significant shielding surrounding the threat object that is not part of the fishing trawler, which further complicates the difficulties with a standoff interrogation source and detector. Eventually, issues concerning AI in maritime environments below the waterline must be addressed, but they are not addressed in this study.

For the purposes of this study, only a single location within the break-bulk cargo carrier ship seen in Fig. 5 was chosen as an AI evaluation location. One of the cargo holds in the forward section of the ship, above the waterline, was modeled using a Cartesian geometry (see Fig. 6), with the representative dimensions and thickness for the hull, floor, and ceiling and interior cargo volume. The cargo hold that was approximated by this simplified geometry is also one of the widest cargo holds, so a threat object placed at the ship's centerline in the geometry would have the maximum amount of shielding available between the threat object and source and detectors. The distance between the side of the break-bulk carrier and the centerline of the ship is 10.5 m. Hence, if a source can

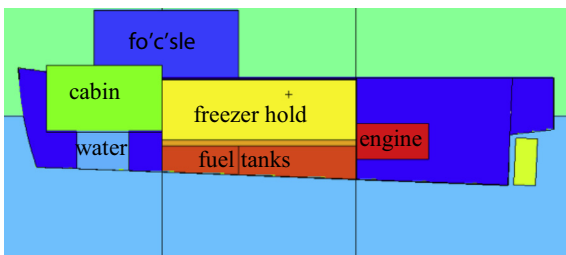


Fig. 4. An elevation view of the fishing trawler MCNPX model with the important compartments identified.

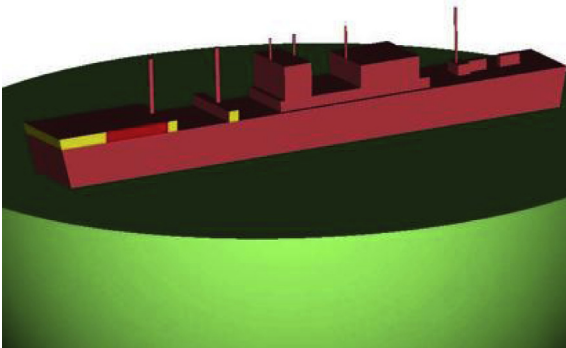


Fig. 5. 3-D view of SS Cape Chalmers MCNPX model.

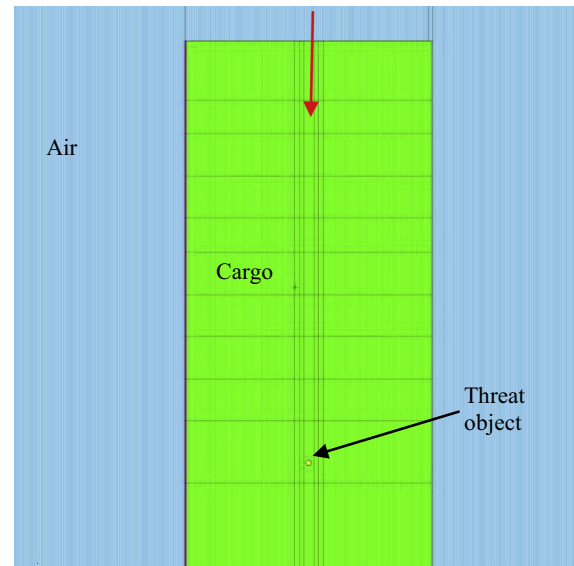


Fig. 6. Plan view of the simplified USS Chalmers cargo hold MCNPX model.

produce a detectable signal in the SNM with this simplified geometry, then the SNM will also be detectable in other areas of the ship. The contents of the cargo hold were modeled as a homogenous mixture distributed throughout hold. Because the use of a homogenized mixture precludes any possible streaming paths, it represents a very conservative approach for both the AI source radiation and the radiation produced by the SNM.

Due to the wide variety of cargos for the cargo hold and more so the variety of structure within the ship itself, the interior region of the simplified model has been represented by four distinct material/shielding configurations, which are shown in Table 1. The cargo loadings in Table 1 were chosen to either represent a physical place where a threat object could be hidden (the fuel tank), or, if the threat object was hidden among cargo, to represent limiting cargo cases. The high-iron cargo would provide greater shielding to photons, and the hydrogenous material would provide greater shielding to neutrons. The DHS cargo is meant to be a mixture of iron and hydrogenous material that would shield both neutrons and photons and is representative of general cargo loadings. The density and composition of the DHS cargo was arrived at by evaluating cargo density and composition data that were reported to the United States Department of Homeland Security (DHS) in Ref. [13].

3. Sources

Numerous sources can be applied in AI scenarios. Table 2 lists a summary of the sources that are considered in this work. The sources in Table 2 are by no means an exhaustive list. They consist of photon sources, neutron sources, and sources that are a mix of neutrons and photons. Source 1 is a standard deuterium–tritium (DT) neutron generator that produces isotropic 14.1-MeV neutrons. Source 2 is a neutron source with energies higher than source 1 that are forward directed, (i.e., not isotropic). Accelerating deuterons to 50 MeV and having them impinge onto a natural Li target produces these neutrons. Some of the deuterons will break-up resulting in neutrons with a wide distribution of energies, some of which will be 50 MeV or higher. Sources 3, 4, and 5 are bremsstrahlung sources with electron energies above 15 MeV. This energy was selected because the peak of the photonuclear cross sections in HEU is between approximately 10 and 15 MeV. Plots

Table 1

Cargo loadings for break-bulk carrier AI analysis.

Cargo material	Density (g/cc)	Description
DHS	0.4000	Represents a mixture of hydrogenous and iron cargo
Diesel	0.9910	Represents threat object placed in a full fuel tank
High Iron	0.6000	Represents a cargo containing mostly iron
Hydrogenous	0.2000	Represents a cargo containing mostly hydrogenous material

Table 2

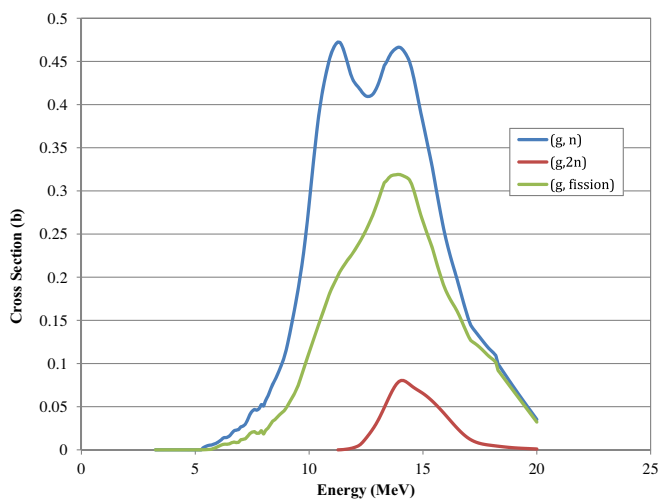
Candidate active interrogation sources.

Source number	Short name	Source description
1	14 MeV n	14 MeV neutrons, (D,T)
2	50 MeV ^2H on Li	High energy neutrons – $^{\text{nat}}\text{Li}(d,n)\text{X}$
3	25 MeV e-/W	25 MeV e- on tungsten, bremsstrahlung
4	50 MeV e-/W	50 MeV e- on tungsten, bremsstrahlung
5	100 MeV e-/W	100 MeV e- on tungsten, bremsstrahlung
6	25 MeV e-/W/ Be	25 MeV e- on tungsten/beryllium, $\gamma + n$
7	50 MeV e-/W/ Be	50 MeV e- on tungsten/beryllium, $\gamma + n$

of pertinent ENDF/B-VII photonuclear cross sections for the HEU threat object is shown in Fig. 7, which includes the total photonuclear cross section (g, n), the cross section for gamma absorption producing two neutrons (g, 2n), and the cross section for gamma-induced fission (g, fission). These cross sections all have peaks between 10 and 15 MeV. Sources 6 and 7 are similar to sources 3 and 4, except downstream from the accelerator converter there is a beryllium target in which some of the bremsstrahlung photons create neutrons from photonuclear interactions, which provide a mixed photon and neutron source.

The MCNPX simulations of the ships being interrogated always started with a photon or neutron source. In other words, the simulations never used electron or deuteron transport because, in general, charged-particle Monte Carlo transport is much slower than neutral-particle Monte Carlo transport.

For the bremsstrahlung sources, the electron beam hitting a block of tungsten was modeled once, and the photons exiting the tungsten were tallied as a function of position, energy, and angle. Similarly, the deuteron beam on the lithium target was simulated once, and the neutrons exiting the lithium were tallied as a

**Fig. 7.** Threat object photonuclear cross sections ENDF/B-VII.0.

function of position, energy, and angle. Of the photons and neutrons that were tallied, a subset of those was included in the bremsstrahlung or neutron spectra that were used in the MCNPX AI simulations. The photons and neutrons included in the AI source spectra were those traveling in the forward direction, $\pm 0.5^\circ$ from the charged particle beam axis, with energy greater than 1 MeV. This does not perfectly model the angular dependence of these sources, but that can only be done if the exact design of a given electron or deuteron accelerator converter and collimator are known. It should be noted that for the bremsstrahlung source the thickness of the tungsten block (converter) was optimized to produce the maximum number of photons with energies of 15 MeV or greater. The plots of the 25-, 50-, and 100-MeV bremsstrahlung spectra that were used are shown in Fig. 8.

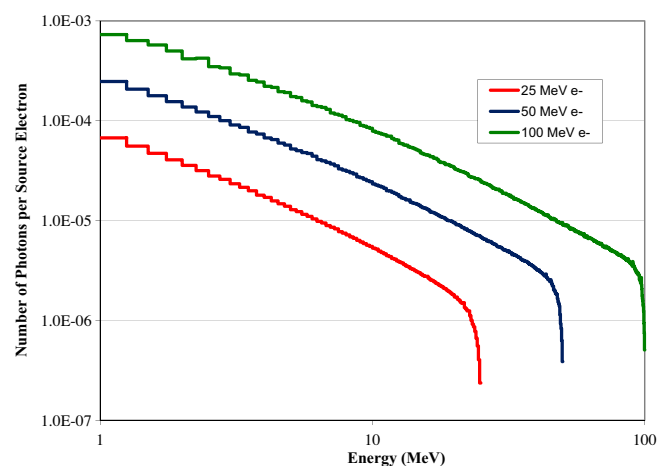
Likewise, the thickness of the lithium target was optimized to produce the maximum number of neutrons with energies between 20 and 35 MeV. Fig. 9 is a plot of the calculated neutron spectrum.

4. Detection signals

In Refs [5,6] and [14] several methods are discussed for detection of HEU during the AI process. Measurement methods include count rates, particle multiplicities, time correlations between multiple detectors, and differential die away. Another measurement method, nuclear resonance fluorescence (NRF), is discussed in more detail in Ref. [15]. The method that appears most readily available, that requires the least amount of development, and that is the simplest to calculate is the measurement of time-dependent count rates between pulses of a pulsed AI source or after a steady-state source is switched off (differential die away that includes prompt and delayed particle detection). Time-dependent count rates are the focus of methods used in this article. The resulting number of particles as a function of time can be compared with and without SNM present to determine whether the AI source is useful. An AI source is considered useful if a difference can be seen in the number of particles as a function of time with and without SNM. The most important difference with time-dependent count rates results from the buildup and detection of delayed-fission neutrons and photons.

4.1. Computational tools

Several different radiation transport codes can be used when evaluating AI sources and techniques. There are a few time-dependent deterministic radiation transport codes that could have been used, but there are no multigroup cross-section libraries that con-

**Fig. 8.** Bremsstrahlung spectra for 25-, 50-, and 100-MeV electrons on tungsten in a forward 1.0-degree cone.

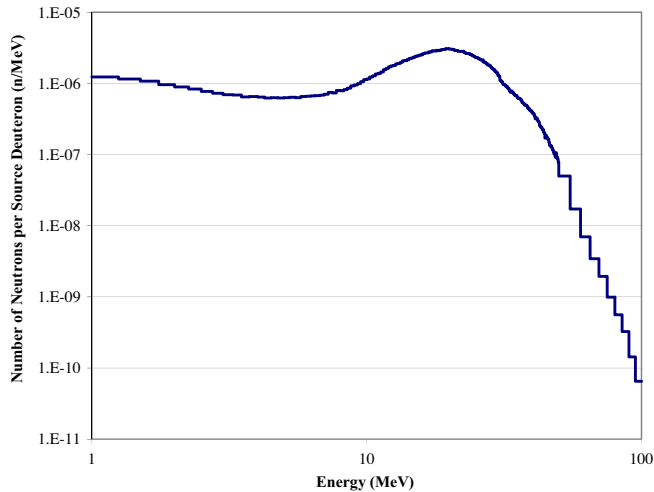


Fig. 9. Neutron spectra for 50-MeV deuterons on lithium in a forward 1.0-degree cone.

tained photonuclear reactions (i.e., up-scatter from photon groups to neutron groups). Ongoing work at Oak Ridge National Laboratory (ORNL) will alleviate this problem in the future, but for this evaluation only Monte Carlo radiation transport codes were available. The primary computational tool of this study is the radiation transport code MCNPX version 2.6.0. Another Monte Carlo code considered was MCNPX-PoliMi [16], which is an excellent code to simulate many of the measurement types discussed in Ref. [14]. MCNPX-PoliMi is useful because it attempts to conserve energy on an event-by-event basis and because all particle production is correlated to the interaction type that produces each particle. However, MCNPX was chosen over MCNPX-PoliMi because MCNPX-PoliMi's post-processing code requires an MCNPX like PTRAC file to be written and analog transport, which precludes the use of parallel processing and simulating deep-penetration shielding calculations, respectively.

A secondary tool, ADVANTG [17,18], was used to generate weight windows and biased sources for MCNPX. ADVANTG was important to all the analyses because the scenarios that are being considered involve geometries that are heavily shielded and not tightly coupled. Therefore, analog (or nearly analog) Monte Carlo calculations will not provide results in a timely fashion and in some cases may not provide any statistically significant results. Ref. [18] provides a few examples of how ADVANTG can be used to accelerate the convergence of Monte Carlo tallies in scenarios similar to those being evaluated by this work.

4.2. Computational methodology

For some of the measurement methods described in Section 4, two measurements are required to definitively detect the presence of SNM: one with the SNM present in the object being interrogated and a second without the SNM present. The difference between the two measurements, Δ , would serve as the actual indication of the presence of SNM.

$$\Delta = \text{Signal_with_SNM} - \text{Signal_without_SNM} \quad (1)$$

In practical applications the two measurements described will not be made. If the object being interrogated is going to be searched so that any SNM can be removed, then no AI measurements are necessary. Therefore, in practical applications it is necessary to have an idea of what the signal without any SNM present would be prior to interrogating the object. How this estimate of the signal without any SNM is arrived at will not be discussed in

detail here. However, here are two suggestions. First, if the material composition and density of the object being interrogated is known, an estimate of the signal could be looked up in a database in which specific signals are correlated with material composition and density and source type. Second, if the material composition and density are unknown and if the object being interrogated is very large, several measurements could be performed to establish a baseline measurement. Any measured signals that do not follow the trends of the baseline measurements might indicate the presence of SNM.

Some methods discussed in Section 4 do not require a measurement with and without any SNM. For example, multiplicity measurements do not require a measurement with and without any SNM because multiplets that deviate from Poisson statistics are an indication of the presence of SNM. However, multiplicities are not being considered in this work because that would require good statistical convergence in multiple detectors for rare events. Instead, the particle count rate (particularly the delayed particle count rate) is being used because it can be calculated with small statistical uncertainties faster than multiplicities and other methods that rely on rare events. The count rates can serve as a good indication of whether or not an AI source can detect the presence of SNM for a given cargo loading by providing a lower bound of the required AI source strength, but may not be the best method for actual application of AI.

Because the method being used to detect the presence of SNM requires two measurements, one with and one without the presence of SNM, it follows that any calculations using that method will also require two calculations, one with and one without the presence of SNM. Each of the MCNPX calculations needs to be a "semi-analog" calculation; "semi-analog" because implicit capture and Russian roulette are used. In other words, neither importances nor weight windows can always be used when the AI source particle is the same species as the particle that, if detected, would indicate the presence of SNM in a given scenario. For example, if the AI source is a DT generator and the interrogation is attempting to detect fission neutrons, MCNPX weight windows can only bias neutrons from the source to the object being interrogated or from the interrogation object to the detector but not both. Work currently under way at ORNL will alleviate this issue in the future [19].

The difference between the total calculated counts with SNM present and without SNM present, Δ , is what indicates whether an AI source can be used to detect the presence of SNM for a given cargo loading. If the calculated count rate with the SNM present is s and the calculated count rate without the SNM present is b_a . The integral of these count rates is S , the total counts with the SNM present, and B_A , the total number of counts without the SNM present or the active background. Therefore, Eq. (1) can be rewritten as Eq. (2),

$$\Delta = \int_0^T S(t)dt - \int_0^T b_a(t)dt = S - B_A, \quad (2)$$

Where T is the total length of time of the AI scan. If S is statistically greater than B_A , or Δ is statistically greater than zero, the specified AI scenario can detect the presence of SNM.

The primary drawback to using two calculations as described in the previous paragraph is that often no importance map or weight windows can be used. Unfortunately, these are two effective variance reduction techniques that are very helpful when geometries are heavily shielded and not tightly coupled. In order to use them, the evaluation would have to be broken down into four calculations instead of two. The four calculations that have to be performed when using weight windows or an importance map are described briefly in the following list.

1. First, weight windows are used to bias AI source particles from the source location to the SNM. The energy and time-dependent leakage of neutrons and photons exiting the SNM are tallied independently. This calculation accurately models fission events in the SNM and transmission of AI source particles through the SNM, and it ensures that the phase space of the SNM is adequately sampled.
2. In calculation 2, the energy- and time-dependent leakage tallies from the first calculation are used as the source. The source particles are biased from the SNM to the detector(s) using weight windows and biased source distributions. The result of the second calculation is the detector response due to the SNM, S_{SNM} . The importance inside the SNM is set to zero so any particles entering the SNM are killed because all particle transport in the SNM was modeled in the first calculation.
3. Calculation 3 is used to obtain the detector response due to the rest of the object being interrogated, S_{OBJ} , or in other words, the signal excluding the SNM. Like calculation 2, in the third calculation the importance inside the SNM is set to zero. The total detector response when SNM is present, S from Eq. (2), is the sum of tallies from calculations 2 and 3.
4. Calculation 4 is used to determine the detector response with no SNM present; i.e., the active background [B_A from Eq. (2)]. The source is the AI source.

These four calculations require that Eq. (2) be modified. Now the total counts when the SNM is present are the sum of tallies from calculations 2 and 3 described above, so Eq. (2) must be rewritten as Eq. (3).

$$\begin{aligned}\Delta &= \int_0^T S_{snm}(t)dt + \int_0^T S_{obj}(t)dt - \int_0^T b_a(t)dt \\ &= S_{SNM} + S_{OBJ} - B_A\end{aligned}\quad (3)$$

4.3. Analysis methodology

The goal of this analysis is to determine what source strength is required for the AI scenario in question to be viable. If the calculation of Δ in Eq. (3) is on a per-source-particle basis, the actual difference between the calculated signal with and without any SNM is $N\Delta$, where N is the source strength. In order to calculate N , some criterion must be established that is used to determine whether $N\Delta$ is significant. Below is a generic criterion that can be used in most cases.

The difference between the signal with and without any SNM present, $N\Delta$, must be greater than z times the standard deviation of the background, σ_B , after T seconds of active interrogation. The background consists of the natural background, B_N , plus the active background, B_A .

Mathematically, that criterion is represented by

$$N\Delta > z\sigma_B \quad (4)$$

or

$$\begin{aligned}N\left(\int_0^T S_{snm}(t)dt + \int_0^T S_{obj}(t)dt - \int_0^T b_a(t)dt\right) \\ > z\sqrt{N\int_0^T b_a(t)dt + \int_0^T b_n(t)dt},\end{aligned}\quad (5)$$

Eq. (5) can be rewritten as Eq. (6) after all the integrations in Eq. (5) are performed.

$$N^2\Delta^2 - Nz^2B_A - z^2B_N \geq 0 \quad (6)$$

The solution for N , keeping the positive root, is shown in Eq. (7).

$$N = \frac{z^2B_A + \sqrt{z^4B_A^2 + 4\Delta^2z^2B_N}}{2\Delta^2} \quad (7)$$

When evaluating N where Δ and B_A are based on a single pulse of a pulsed AI source or for a steady-state source, N will be the total number of AI source particles needed over the full interrogation time, T . If the MCNPX source represents one pulse of a pulsed AI source when calculating Δ and B_A , then the calculated time-dependent detector response, counts in this case, only represents the response due to a single source pulse. To accurately calculate Δ and B_A due to a pulsed AI source the superposition of the detector response due to each source pulse over the interrogation time must be convolved with a function that represents the pulsed nature of the source and detector over the interrogation time. If this superposition and convolution are not performed the buildup of delayed particles intermingled with the bursts of prompt particles will not be accurately modeled, so this is vital for pulsed AI sources.

Further consideration of Eq. (7) is warranted because a Monte Carlo code is the primary tool used in these analyses. For Eq. (7), the limit of N as Δ goes to zero is infinity. Physically that corresponds to the fact that as the difference between the signal with and without any SNM, Δ , decreases the required AI source strength, N , must increase to meet the criterion prescribed in Eq. (4). The true value of Δ must always be greater than or equal to zero because when no SNM is present, or if it is undetectable, the true value of S_{SNM} plus the true value of S_{OBJ} will equal the true value of B_A . The calculated value of Δ may be less than zero or statistically indistinguishable from zero, but that is purely due to the statistical uncertainty associated with the MCNPX solution. For Δ to be positive and statistically distinguishable from zero, the following criterion must be met:

$$\Delta > y\sigma_\Delta, \quad (8)$$

where, S_{OBJ} , S_{SNM} , and B_A are assumed to be uncorrelated, σ_Δ is

$$\sigma_\Delta = \sqrt{\sigma_{SNM}^2 + \sigma_{OBJ}^2 + \sigma_{B_A}^2}. \quad (9)$$

The criterion in Eq. (8) looks very similar to the criterion in Eq. (4), but it is actually quite different. In Eq. (8), σ_Δ does not include the uncertainty of the natural background. The parameter y in Eq. (8) has the same meaning as z in Eq. (4); Δ must be y standard deviations above zero. In Eqs. (4) and (8), y and z do not have to equal the same value. N is not included in Eq. (8) because this criterion can be evaluated on a per-source-particle basis. Once the criterion in Eq. (8) is met, the criterion in Eq. (4) can be applied and Eq. (7) can be used to calculate the required source strength for the given AI scenario.

An interesting question is, “what should be done if the criterion in Eq. (8) is not met?” The most straightforward answer is that the MCNPX calculations must be continued in order to reduce the statistical uncertainty. However, in many cases further reduction of the Monte Carlo statistical uncertainties may not be practical. If the criterion in Eq. (8) has not been met and the Monte Carlo statistical uncertainties are small, then the following approximation for Δ can be used in Eq. (7):

$$\Delta_{approx} = S_{SNM}. \quad (10)$$

Essentially, Eq. (10) says that if the criterion in Eq. (8) cannot be met, then it can be assumed that Δ is simply equal to the signal from the SNM. Neglecting the B_A and S_{OBJ} is not a bad approximation when S_{SNM} is a small fraction of the total AI signal, S , and S_{OBJ} is nearly equal to B_A . Given Eqs. (3) and (7) and the fact that the true value of S_{OBJ} is always less than or equal to the true value of B_A , the true value of Δ is always less than or equal to the true value of S_{SNM} . Therefore, Δ is always less than or equal to Δ_{approx} . This

means the approximation to Δ in Eq. (10) always results in a calculated value of the required AI source strength, N , which is less than or equal to the true value of N . So if the Monte Carlo results for S_{SNM} , S_{OBJ} , and B_A have small statistical uncertainty, but Δ is statistically indistinguishable from zero, Δ_{approx} can be used to calculate a lower bound for N . Once a lower bound of N is known, one can decide whether the Monte Carlo uncertainties for S_{SNM} , S_{OBJ} , and B_A need to be further reduced. If the lower bound of N represents an AI source strength that is achievable, then those uncertainties need to be reduced to more accurately calculate N . However, if the lower bound of N is unachievable, then further refinement of the Monte Carlo uncertainties is unwarranted.

5. Active interrogation source investigations

Calculations have been performed to determine which AI techniques would represent viable options for the ship-to-ship maritime scenario. First, fission rate per source particle results within the HEU are reported. Next, some particle counts rates calculated using the idealized computational detector described below are presented. Then the required source strengths for some of the sources in Table 2, based on the count rate results, are presented.

In the calculations discussed in the following sections, the AI sources and particle detector tallies are co-located 10 m from the hull of the ship. No actual detectors are modeled. The detector tallies are based on surface tallies over a $1 \times 1 \text{ m}^2$ area, which are 100% efficient. These results can be applied to any detector if the results are scaled to account for the different detector area (size of detector) and a fluence-to-detector response function is applied, which is more accurate if the fluence (counts) and detector response function are a function of energy. Details about realistic detectors are available in Refs. [5] and [6]. The methodology discussed in Section 5 is applied here in Section 6.

5.1. Fission rate results: yacht and trawler

The fission rates due to the sources in Table 2 were calculated for the HEU threat object in the fishing trawler and luxury yacht locations described in Section 2. In each calculation the axis of the source always passes directly through the center of the threat object, so the sources are always at the same height above the waterline and at the same position along the keel of the ship as the threat object. This is an important assumption because this condition will occur very rarely due to the relative motion of two ships at sea. The total fission rate per source particle results (neutron induced plus photon induced) for the different threat object locations are presented in Table 3. The Monte Carlo relative uncertainties for all the results in Table 3 are less than 2%.

5.2. Detection of fission particle results: yacht and trawler

Next, the time and energy dependence of photons and neutrons entering the front face of a detector were tallied. These tallies represent the detector response due to the SNM, S in Eq. (2) or S_{SNM} plus S_{OBJ} in Eq. (3). In this section only results for the bremsstrahlung sources (without beryllium) are discussed because the results presented in Table 3 show that those sources produce the highest fission rate per source particle. Representative samples of simulated time-dependent detector responses are shown. For comparison purposes, the detector response without any SNM is presented alongside the results when SNM is present. No energy-dependent responses are shown because it is well known that energy spectra are not always reliable when looking to detect the presence of SNM. For example, lead and depleted uranium under the right conditions can produce similar energy spectra [20]. Time-dependent results are useful be-

cause fission chain reactions will produce additional neutrons and photons. Plus, the fission products produced during the fission chains decay and subsequently produce delayed neutrons. All materials have the potential to create delayed photons via activation and/or decay of fission products. Delayed photons can also be produced by inelastic scattering or radiative capture of delayed neutrons. Excluding activation photons, all the delayed particles produced result somehow from a fission event that occurs as part of a fission chain reaction, which further emphasizes the importance of the delayed particles to signal the presence of any SNM.

Figs. 10 and 11 show the time-dependent neutron and photon detector responses due to the 50-MeV bremsstrahlung source when the threat object is 1 m from the hull inside the luxury yacht cabin, which is the scenario that produced the highest fission rate in the luxury yacht. The lowest fission rate for the luxury yacht with a bremsstrahlung source (without Be) occurred when the threat object was along the luxury yacht centerline inside the liquid storage tank during interrogation with the 25-MeV bremsstrahlung source. Figs. 12 and 13 show the time-dependent neutron and photon detector responses for this scenario. Figs. 10–13 show the time-dependent detector response for only a single source pulse, and the plotted results are per source photon (at this point in the analysis the required number of photons and electrons is unknown). The Monte Carlo relative uncertainties for most of the time bins in Figs. 10–13 are less than 10%. However, at later times ($>1 \times 10^{-2}$ s) the uncertainties increase, but are all less than 20%.

There are two vertical dotted lines in Figs. 10–13 that provide information about the plotted detector responses with respect to the repetition rate of the AI source and the pulse width. In these calculations it was assumed that the AI source pulsed at 60 Hz and that each pulse lasted for 4 μs . The first dotted line, on the left side of these figures, marks the end of the first source pulse. While the second dotted line, on the right, marks the beginning of the second pulse. It is impossible to look at Figs. 10–13 and make any quantitative assessment about the source strength required to detect the presence of SNM. However, a qualitative assessment can be made. The signal with and without the SNM must diverge at some time in these figures in order to detect the presence of SNM. Therefore, the scenario plotted in Figs. 10 and 11 can definitely detect the presence of SNM, while the scenario in Figs. 12 and 13 most likely cannot. The question now is what source strength is required to detect the differences in Figs. 10 and 11, and is that source strength reasonably achievable?

5.3. Required active interrogation source strengths: yacht and trawler

The required source strengths for the sources and scenarios that have been analyzed for the luxury yacht and fishing trawler are presented next. They have been limited to the bremsstrahlung sources and are reported with units of electrons per second on a tungsten converter, without beryllium, based on the fission rate data presented in Table 3. Eq. (7) is used to calculate the required source strength. The criterion for successfully detecting the SNM is as follows:

The difference between the signal with and without any SNM present, $N\Delta$, must be greater than 5 times the standard deviation of the background, σ_B , after 100 s of active interrogation. The background consists of the natural background, B_N , plus the active background, B_A . It is assumed that the natural background is 10 neutrons per second and 100 photons per second.

Assuming a neutron background of 10 neutrons per second is high for sea level background outdoors closer to the equator than either of the poles, but is not an unrealistic estimate inside a building or ship at higher latitudes [5,21–23]. The photon background at sea will be less than the photon background on land, particularly in the presence of some stone and brick buildings. A photon back-

Table 3

Fission rates inside the threat object while in the luxury yacht and fishing trawler freezer hold (10 m standoff – fissions per source electron or neutron)^a.

Source	Yacht cabin, centerline	Yacht cabin, 1 m from hull
25 MeV e-/W	3.88E-03	7.37E-03
25 MeV e-/W/Be	2.81E-03	5.32E-03
50 MeV e-/W	4.98E-03	9.32E-03
50 MeV e-/W/Be	3.55E-03	6.63E-03
14 MeV n	2.84E-05	7.02E-05
Source	Yacht water storage tank, centerline	Yacht water storage tank, 1 m from hull
25 MeV e-/W	8.19E-05	5.07E-03
25 MeV e-/W/Be	6.00E-05	3.48E-03
50 MeV e-/W	1.52E-04	7.16E-03
50 MeV e-/W/Be	1.12E-04	5.17E-03
100 MeV e-/W	3.28E-04	***
14 MeV n	5.93E-08	1.50E-06
50 MeV ² H on Li	6.54E-06	***
Source	Yacht engine room, centerline	Yacht engine room, 1 m from hull
25 MeV e-/W	2.36E-04	2.90E-03
25 MeV e-/W/Be	1.70E-04	2.09E-03
50 MeV e-/W	3.14E-04	4.31E-03
50 MeV e-/W/Be	2.29E-04	2.73E-03
14 MeV n	1.76E-05	6.31E-05
Source	Trawler freezer, centerline	Trawler freezer, 1 m from hull
25 MeV e-/W	3.84E-04	9.12E-03
25 MeV e-/W/Be	2.78E-04	6.90E-03
50 MeV e-/W	5.85E-04	1.25E-02
50 MeV e-/W/Be	4.41E-04	9.32E-03
14 MeV n	1.25E-09	1.09E-04

***This source was not evaluated for this location.

^a Monte Carlo relative uncertainties all less than 2%.

ground of 100 counts per second is reasonable compared to photon backgrounds on land near sea level. This photon background is an overestimate inside a ship at sea but not a ship dockside [6,22,23]. It is important to this type of analysis to not grossly overestimate or underestimate the background radiation. Underestimating the background will make it easier for the proposed AI scenarios to successfully detect SNM, and therefore require smaller AI source strengths, while overestimating the background will make things more difficult for the proposed AI scenarios.

For the superposition and convolution that must be performed to compensate for the fact that MCNPX modeled a single pulse of the AI sources, it is assumed that all the sources are pulsed with a repetition rate of 60 Hz and that the pulse width, also detector downtime, is 4 μ s. Fig. 14 shows the required source strengths based on the neutron detector responses. Fig. 15 shows the required source strengths based on the photon detector responses. The cases marked “centerline” in Figs. 14 and 15 have the threat object along the centerline of the ship; the cases marked “hull” have the threat object 1 m inside the hull of the ship. The Monte Carlo relative uncertainty for all the source strengths shown in Figs. 14 and 15 are less than 10%. In the luxury yacht, all the cases with the threat object along the centerline of the liquid storage tank (water tank) are statistically indistinguishable, i.e., Eq. (8) was not satisfied with y equal 2 and the approximation in Eq. (10) was applied. The same is also true when the threat object is along the centerline of the freezer hold in the fishing trawler. Therefore, the source strengths shown for the yacht water tank and trawler freezer hold, with the threat object along the centerline, are lower estimates of the required source strength.

5.4. Required active interrogation source strengths: break-bulk cargo carrier

Based on the results of the AI scenarios analyzed for the luxury yacht and fishing trawler, it is obvious that the AI scenarios for the

break-bulk carrier will be very challenging. For the luxury yacht and the fishing trawler the maximum amount of shielding was a few meters, but the maximum amount of shielding for a break-bulk carrier is much more likely to be tens of meters. The placement of the threat object for this analysis can be seen in Fig. 6, and the shielding materials are listed in Table 1. The sources used in the break-bulk carrier scenarios were limited to the bremsstrahlung sources without beryllium. The methodology and superposition and convolution described in Section 4 and the detection criterion and source repetition rate described in Section 5.3 were applied to the break-bulk carrier as well. All these cases place the threat object at the centerline of the break-bulk carrier. The most significant difference between the break-bulk carrier and the other ships is that the sources were only 1 m from the hull of the ship. Fig. 16 shows the required source strengths based on the neutron detector responses.

6. Conclusions and summary

The fission rate results in Table 3 show that the bremsstrahlung sources without any beryllium produce the largest number of fissions per second. This is partly due to the ability of the high-energy photons (>20 MeV) to more easily penetrate shielding materials and to reach the threat object. Once a few neutrons from photonuclear interactions have been created in the threat object, they can stimulate fission chains and create additional fission neutrons. This is particularly evident when the threat object is in the fishing trawler freezer hold, 1 m inside the hull. In this case there is not a large amount of shielding material between the source and threat object, and the contents of the freezer hold provide a reflector and moderator for the neutrons that leak from the threat object. Although neutrons can penetrate high-Z materials much more easily than photons, the bremsstrahlung sources always outperformed the DT neutron source. The neutron sources do not perform as well as the bremsstrahlung sources because they are isotropic, like

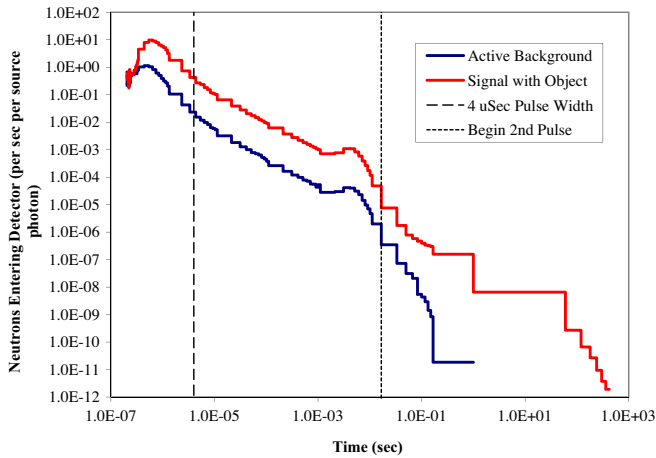


Fig. 10. Comparison between neutron signals with and without the threat object located in the luxury yacht cabin 1 m inside the hull.

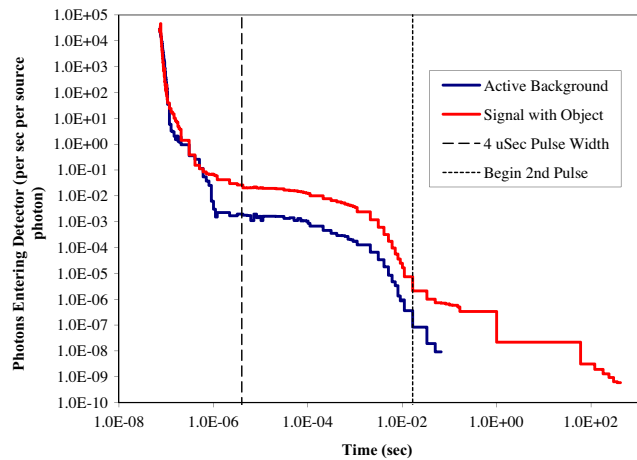


Fig. 11. Comparison between photon signals with and without the threat object located in the luxury yacht cabin 1 m inside the hull.

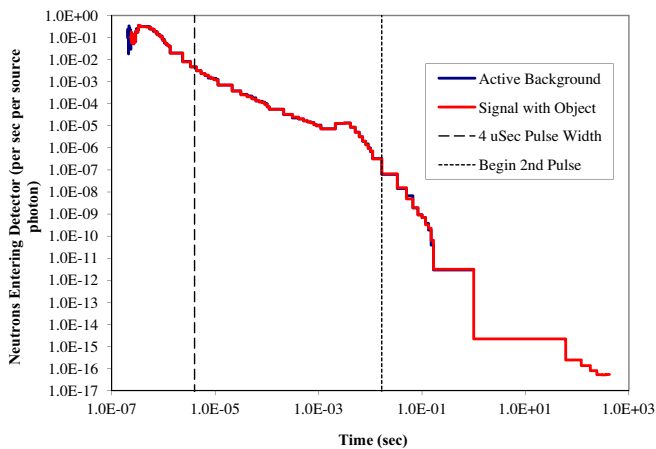


Fig. 12. Comparison between neutron signals with and without the threat object located in the luxury yacht liquid storage tank along the centerline of the yacht.

perform as well as the bremsstrahlung sources alone. The photons that are absorbed in the beryllium to create neutrons end up creating neutrons in an isotropic manner. Based on these results, it was decided to focus on bremsstrahlung sources for the rest of this analysis. Isotropic sources may be useful when systems are tightly coupled, possibly even if the tightly coupled system has many mean free paths of shielding. However, for any standoff AI scenario, directional sources must be used.

Figs. 10–13 show the extremes of the detection signals for the interrogation scenarios with bremsstrahlung sources. For the best cases there is a distinct difference between the signal with and without the threat object present. In the worst cases the signals are nearly indistinguishable. The differences seen in Figs. 12 and 13 are primarily due to statistical uncertainty.

The results of most interest from this analysis are the electron intensities (or source strengths) required to detect an HEU threat object after a 100 s AI scan in Figs. 14–16. The best case, i.e., the lowest source strength, is the lowest density case, the yacht cabin. The yacht engine room requires a source strength that is larger than the cabin, and the yacht liquid storage tank requires an even larger interrogation source. The largest required source strength amongst the yacht and trawler scenarios is when the threat object is at the center of the fish hold in the trawler. However, when the threat object is moved within 1 m of the fishing trawler hull the re-

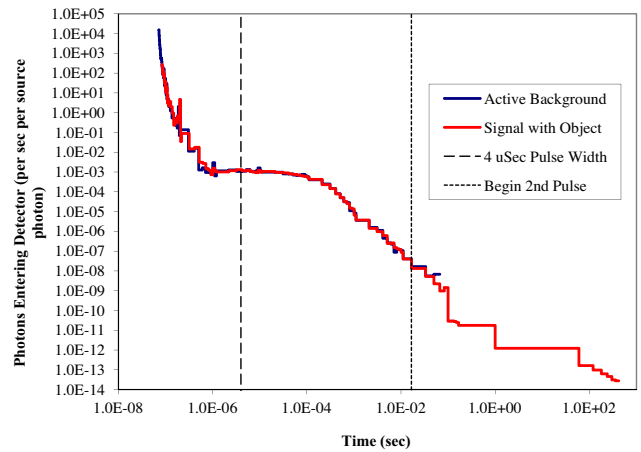


Fig. 13. Comparison between photon signals with and without the threat object located in the luxury yacht liquid storage tank along the centerline of the yacht.

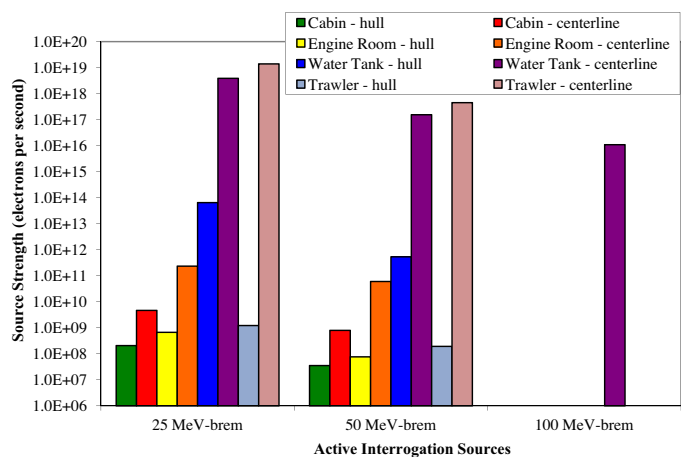


Fig. 14. Electron accelerator intensity required to meet the criterion for successfully detecting SNM via the production of neutrons in the given luxury yacht and fishing trawler scenarios.

the DT source. The directional dependence of the bremsstrahlung sources is very forward peaked, so most of the bremsstrahlung photons travel towards the threat object. This is also why the bremsstrahlung–beryllium mixed neutron photon sources do not

quired electron source intensity is greatly decreased. At this position in the trawler freezer hold, there is only about 13 cm of the fish and ice mixture between the threat object and detector. The increased fission rate mentioned previously in this section combined with the lack of attenuation of the detection signal results in easy detection when the threat object is near the hull of the fishing trawler. In order to put the numbers in Figs. 14–16 in perspective, they can be compared to the accelerator in Ref. 4 that operated with a beam current between 3 and 4 μA ($\sim 1.0 \times 10^{13}$ electrons per second).

An interesting result was that in nonhydrogenous shielding scenarios the required source strength was fairly similar regardless of whether neutrons or photons were being detected during the interrogation (within an order of magnitude). However, in the hydrogenous cases the source strength required for the detection of neutrons is much larger than that required to detect photons because hydrogenous material does not attenuate photons as well as it attenuates neutrons. If a case were analyzed that had a much larger volume fraction of high-Z material, a similar result might be observed where the source strength increase is smaller for detecting neutrons than for detecting photons. This illustrates the need

for interrogation techniques that can effectively measure neutrons and photons.

For the break-bulk carrier, standoff AI is practically impossible. Some scenarios may exist that successfully detect SNM in a break-bulk carrier; such as if the threat object was 1 m inside the hull. However, it is not realistic to expect standoff AI to work with any high degree of reliability because the break-bulk carrier is such a large class of ship and because it can carry large quantities of cargo that provide shielding.

This analysis has shown that standoff AI is possible in the maritime environment if a number of criteria are met. First, the standoff distances cannot be too large, which in this context is less than 10s of meters. Second, highly efficient detectors are needed. This analysis modeled 100% efficient detectors, but realistic detectors would increase the required source strength by a factor between 2 and 100 [5 and 6]. Third, the interrogation source is highly directional (not isotropic). Fourth, the SNM is not too heavily shielded. Fifth, the natural background is well accounted for. Significant increases or decreases in the background source strength will increase or decrease the required AI source strength, respectively. Finally, the interrogation source is directed exactly at the SNM. This final point is very significant considering the relative motion of two ships at sea and that the threat object fission rate, and subsequently S_{SNM} , decrease as the AI source moves away from the SNM. Furthermore, this analysis has relied on a methodology that compares interrogation signals with and without any SNM present, which is not realistic in normal conduct of operations. In short, all these criteria point to very optimistic evaluations of source strengths required to perform AI.

An important fact about the detection of SNM via AI and the detection of fission neutrons and photons is that no matter how fission is induced, the signal from fission will always be the same; i.e., particles will be emitted isotropically, and the spectrum of those particles will be the same for a given material. Therefore, whatever AI source is used to induce fission, the signal that must be detected will always be the same and will always suffer from the same problems. In light of this, it does not seem practical to develop new exotic sources for AI that can induce fission from great distances or when the SNM is surrounded by a large amount of shielding. If the shielding is sufficient enough to prevent neutrons and photons from sources already typically available, like those in Table 2, from reaching the SNM then that shielding will also be able to prevent fission neutrons and photons from reaching a detector. Simply increasing the AI source strength and/or energy in order to increase the fission rate also leads to larger power demands and shielding requirements to operate the AI source, which can lead to that source being impractical, especially in the maritime environment. Time and funding should be focused on efforts to increase our ability to detect fission sources at greater distances and when those sources are heavily shielded, to reduce the active background generated by an AI source, or to investigate signatures other than fission as a means to detect the presence of SNM.

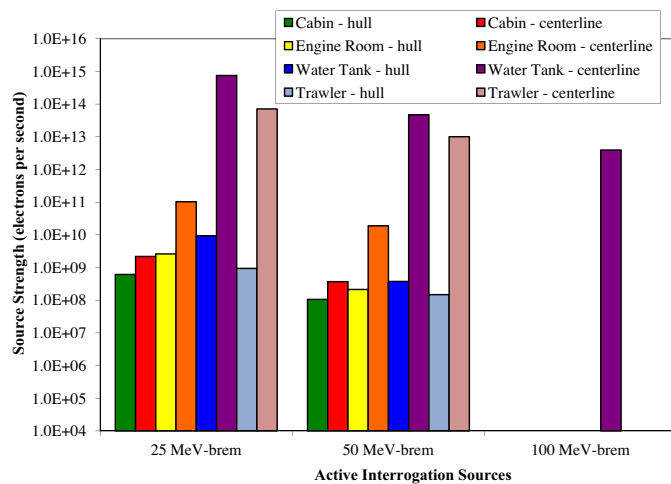


Fig. 15. Electron accelerator intensity required to meet the criterion for successfully detecting SNM via the production of photons in the given luxury yacht and fishing trawler scenarios.

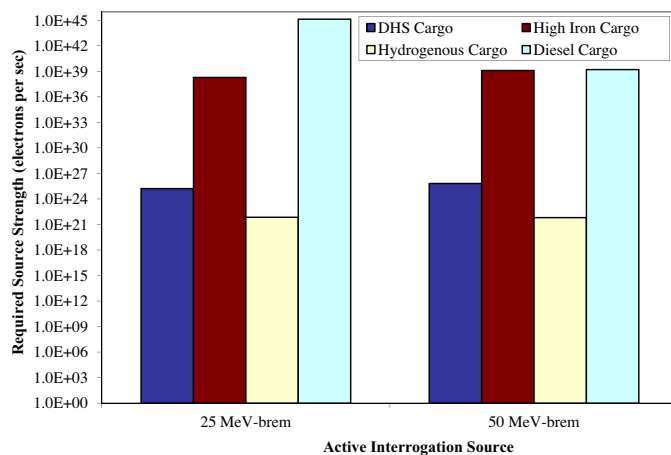


Fig. 16. Electron accelerator intensity required to meet the criterion for successfully detecting SNM via the production of neutrons in the break-bulk carrier scenarios.

Acknowledgements

The authors would like to thank L. Waters and J. Elson of Los Alamos National Laboratory for providing their original fishing trawler model to us.

This research is supported by the National Nuclear Security Administration, Defense Nuclear Nonproliferation, Office of Nonproliferation and Verification Research and Development under contract with UT-Battelle, LLC.

References

- [1] C.E. Moss et al., Comparison of active interrogation techniques, *IEEE Trans. Nucl. Sci.* 53 (2006) 2242–2246.
- [2] B.W. Blackburn et al., Utilization of actively-induced, prompt radiation emission for nonproliferation applications, *Nucl. Instrum. Meth. B* 261 (2007) 341–346.
- [3] J.W. Sterbentz et al., Benchmark validation comparisons of measured and calculated delayed neutron detector responses for a pulsed photonuclear assessment technique, *Nucl. Instrum. Meth. B* 261 (2007) 373–377.
- [4] J.L. Jones et al., Detection of shielded nuclear material in a cargo container, *Nucl. Instrum. Meth. A* 562 (2006) 1085–1088.
- [5] R.C. Runkle, A. Bernstein, P.E. Vanier, Securing special nuclear material: recent advances in neutron detection and their role in nonproliferation, *J. Appl. Phys.* 108 (2010) 111101.
- [6] R.C. Runkle, L.E. Smith, A.J. Peurrung, The photon haystack and emerging radiation detection technology, *J. Appl. Phys.* 106 (2009) 041101.
- [7] IAEA Safeguards Glossary 2001 Edition, International Nuclear Verification Series No. 3, International Atomic Energy Agency, Vienna, Austria (2002).
- [8] D. Pelowitz (Ed.), MCNPX user's manual version 2.6.0, Los Alamos National Laboratory, LA-CP-07-1473 (2008).
- [9] <http://www.oceanalexander.com>.
- [10] <http://www.starkbros.co.nz>.
- [11] Private Communication, Julia Klaus, United States Coast Guard Federal Law Enforcement Training Center, April 30, 2008.
- [12] Private Communication, Jay Elson, Los Alamos National Laboratory, May 29, 2008.
- [13] L.E. Smith et al., Viability Study for In-Transit Screening of Maritime Cargo: Final Report, PNNL-17780, Pacific Northwest National Laboratory, Richland, Washington, 2008.
- [14] J.T. Mihalczko, Radiation detection for active interrogation of HEU, ORNL/TM-2004/302, Oak Ridge National Laboratory, Oak Ridge, Tennessee, 2004.
- [15] W. Bertozzi et al., Nuclear resonance fluorescence and effective Z determination applied to detection and imaging of special nuclear material, explosives, toxic substances, and contraband, *Nucl. Instrum. Meth. B* 261 (2007) 331–336.
- [16] E. Padovani et al., MCNPX-PoliMi User's Manual, Polytechnic of Milan, Italy, University of Michigan, Ann Arbor, MI, 2012.
- [17] J.C. Wagner, An automated deterministic variance reduction generator for Monte Carlo shielding applications, Proceedings of the American Nuclear Society 12th Biennial RPSD Topical Meeting, Santa Fe, New Mexico, 2002. April 14–18.
- [18] S.W. Mosher et al., Automated weight-window generation for threat detection applications using ADVANTG, Proceedings of the International Conference on Mathematics, Computational Methods & Reactor Physics (M&C 2009), Saratoga Springs, New York, 2009. May 3–7.
- [19] D.E. Peplow, T.M. Evans, J.C. Wagner, Simultaneous optimization of tallies in difficult shielding problems, *Nucl. Energ.* 168 (2009) 785–792.
- [20] B. Blackburn et al., Detection of special nuclear material by means of promptly emitted radiation following photonuclear stimulation, 2007 IEEE Nuclear Science Symposium, Honolulu, Hawaii, 2007. October 28–November 3.
- [21] P. Goldhagen, Source Standards – Natural Radiation and Cosmic Rays, 2008 Workshop on Radiation Transport Simulation Methodology for Threat Reduction Applications, Los Alamos, New Mexico, (2008), November 18–19.
- [22] D. J. Mitchell, G. Lasche, and J. Mattingly, Calculation of Radiation Backgrounds, 2008 Workshop on Radiation Transport Simulation Methodology for Threat Reduction Applications, Los Alamos, New Mexico, (2008), November 18–19.
- [23] D. L. Dunn, et al. Maritime Background Radiation Program (MBRP) Phase I Final Report, SRNL-NHS-2006-00007, Rev. 2, Savannah River National Laboratory, Aiken, South Carolina (2006).